



Invited Article: A rigid coherent anti-Stokes Raman scattering endoscope with high resolution and a large field of view

Cite as: APL Photonics 3, 092409 (2018); <https://doi.org/10.1063/1.5027182>

Submitted: 28 February 2018 . Accepted: 16 May 2018 . Published Online: 02 August 2018

P. Zirak, G. Matz, B. Messerschmidt, T. Meyer, M. Schmitt , J. Popp , O. Uckermann, R. Galli, M. Kirsch, M. J. Winterhalder, and A. Zumbusch 

COLLECTIONS

Paper published as part of the special topic on [Biomedical Photonics](#) and [Coherent Raman Spectroscopy and Imaging](#)



View Online



Export Citation



CrossMark

ARTICLES YOU MAY BE INTERESTED IN

[Perspective: Coherent Raman scattering microscopy, the future is bright](#)

APL Photonics 3, 090901 (2018); <https://doi.org/10.1063/1.5040101>

[Invited Article: Label-free nerve imaging with a coherent anti-Stokes Raman scattering rigid endoscope using two optical fibers for laser delivery](#)

APL Photonics 3, 092407 (2018); <https://doi.org/10.1063/1.5031817>

[Invited Article: Comparison of hyperspectral coherent Raman scattering microscopies for biomedical applications](#)

APL Photonics 3, 092404 (2018); <https://doi.org/10.1063/1.5030159>

APL Photonics
Special Topic on Biomedical Photonics

READ NOW!

Invited Article: A rigid coherent anti-Stokes Raman scattering endoscope with high resolution and a large field of view

P. Zirak,^{1,a} G. Matz,^{2,a} B. Messerschmidt,² T. Meyer,^{3,4} M. Schmitt,⁴ J. Popp,^{3,4} O. Uckermann,⁵ R. Galli,⁶ M. Kirsch,⁵ M. J. Winterhalder,¹ and A. Zumbusch¹

¹Department Chemie and Center for Applied Photonics, University of Konstanz, 78457 Konstanz, Germany

²GRINTECH GmbH, Schillerstr. 1, 07745 Jena, Germany

³Leibniz Institute of Photonic Technology, Albert-Einstein-Str. 9, 07745 Jena, Germany

⁴Institute of Physical Chemistry and Abbe Center of Photonics, Friedrich Schiller University Jena, Albert-Einstein-Str. 6, 07745 Jena, Germany

⁵Neurosurgery, University Hospital Carl Gustav Carus, Technische Universität Dresden, 01307 Dresden, Germany

⁶Clinical Sensing and Monitoring, Anesthesiology and Intensive Care Medicine, Faculty of Medicine, Technische Universität Dresden, 01307 Dresden, Germany

(Received 28 February 2018; accepted 16 May 2018; published online 2 August 2018)

Nonlinear optical endoscopy is an attractive technique for biomedical imaging since it promises to give access to high resolution imaging *in vivo*. Among the various techniques used for endoscopic contrast generation, coherent anti-Stokes Raman scattering (CARS) is especially interesting. CARS endoscopy allows molecule specific imaging of unlabeled samples. In this contribution, we describe the design, implementation, and experimental characterization of a rigid, compact CARS endoscope with a spatial resolution of 750 nm over a field of view of roughly 250 μm . Omission of the relay optics and use of a gradient index lens specifically designed for this application allow one to realize these specifications in an endoscopic unit which is 2.2 mm wide over a length of 187 mm, making clinical applications during surgical interventions possible. Multimodal use of the endoscope is demonstrated with images of samples with neurosurgical relevance. © 2018 Author(s). All article content, except where otherwise noted, is licensed under a Creative Commons Attribution (CC BY) license (<http://creativecommons.org/licenses/by/4.0/>). <https://doi.org/10.1063/1.5027182>

INTRODUCTION

Nonlinear optical microscopy has become a standard tool for *in vivo* investigations in cell biological and biomedical settings. While the most prominent among these approaches is two-photon excited fluorescence microscopy (TPEF),⁹ also methods like second and third harmonic generation (SHG and THG) microscopy,^{13,7,2,8} as well as coherent anti-Stokes Raman scattering (CARS)^{11,36} and stimulated Raman scattering (SRS)^{28,12,27} microscopy, are routinely employed. A common feature of all nonlinear optical microscopy methods is their inherent three-dimensional imaging capability. Since efficient nonlinear excitation is only possible with very high electric fields, in all practical implementations, nonlinear optical excitation processes require the use of short laser pulses for excitation. Even then, the excitation is restricted to the focal region which allows the generation of three dimensional images of molecular distributions by raster scanning the sample. Having said that, the different techniques can, however, be distinguished based on the manner in which contrast is generated. As a third order nonlinear process, THG does not pose specific symmetry constraints on signal generation and any isotropic medium will give a certain signal proportional to the materials' third

^aP. Zirak and G. Matz contributed equally to this work.

order nonlinear optical susceptibility $\chi^{(3)}$. In practice, THG is used for *in vivo* imaging of unlabeled lipids which exhibit a very strong $\chi^{(3)}$.^{8,35} SHG, by contrast, requires a symmetry break in the medium for efficient signal generation. Due to this restriction, SHG microscopy provides an excellent means to investigate noncentrosymmetric biological structures such as collagen with high sensitivity and low sample background.⁷ Different from the two latter methods, TPEF microscopy and coherent Raman microscopy offer the possibility to generate contrast with molecular specificity. In the case of TPEF, this commonly requires the labelling of the sample with suitable fluorophores. Under this condition, TPEF gives molecule specific contrast, which is not the case if autofluorescence of the sample is exploited, an approach often used in applications in which different imaging modalities are combined. The molecule specific contrast generation in unlabeled samples is the realm of the coherent Raman microscopy methods based on CARS and SRS. In both methods, the vibrational resonances of the sample molecules are directly used to generate contrast.

Following the introduction of the different nonlinear optical microscopy techniques, also numerous adaptations of these to endoscopic imaging have been reported. While in endoscopy it is not necessary to generate three-dimensional images, the most important advantage of employing nonlinear optical processes in endoscopy is the restriction of the imaging to a well-defined focal plane. The price to be paid for this attractive feature is the necessity to generate an image by raster scanning and the requirement of delivering sufficiently short laser pulses to the focus. A lot of work has thus been dedicated to miniaturizing sample scanning devices such that they can be realized using a typical endoscope diameter of a few mm^{31,26,14,21,32} and to the development of efficient schemes for laser pulse delivery.^{20,1,6,22} With respect to the sample scanning, three different strategies have been followed in the past. The first approach consists in scanning one end of an optical fiber bundle containing several tens of thousands of individual fibers. The one-to-one relation between the fibers at both ends of the bundle then allows the generation of an optical image in which each pixel corresponds to the intensity recorded by one optical fiber element.^{19,15,23} While this approach holds great promise for the design of flexible endoscopes, the achievable image quality to date is limited by the number of optical fibers in the bundle. High resolution images are more easily obtained by using conventional scanning devices based on either piezo or galvanometer scanners. In this case, the problem consists in the miniaturization of the device. Scanners with a diameter of less than 2 mm can be realized by fixing the end of the optical fiber used for laser pulse delivery to a piezo scanner. Images are generated by scanning the end of the fiber in front of a lens which focuses the excitation light onto the sample.^{29,10} This approach allows the generation of images with spatial resolutions comparable to those of nonlinear optical microscopes. Future applications of this method in medical environments might, however, be hampered by the fact that the piezo device, which is positioned in close proximity to the sample, requires a comparatively high voltage supply. Therefore, the placement of the actual scanning unit far from the sample environment has been pursued in a number of experimental designs. Scanning is then most often achieved by a galvanometer scanner which scans the excitation laser beam in *xy* over a scan lens which has a focal plane in common with a tube lens. The tube lens produces a collimated beam which is finally focused onto the sample with a microscope objective.¹⁷ The technical challenge in this approach is the miniaturization of all components to fit into dimensions typical for an endoscope. No matter whether piezo or galvanometer scanning is employed, it is necessary that the last optics which focuses the excitation light onto the object has a small diameter. Therefore, gradient index (GRIN) lenses have been used in the vast majority of nonlinear optical endoscopes reported to date. GRIN lenses have two planar surfaces, and focusing is achieved by precise control of the refractive index profiles within the glass slab, which is achieved by controlled diffusion of ions into the glass.²⁵ GRIN optics can be designed as compound objectives such that despite their small diameters in the mm range, excellent imaging properties even for high numerical apertures can be realized.³

In this contribution, we report the design and experimental characterization of a novel rigid endoscope suited for CARS imaging. In order to allow future applications in neurosurgical interventions, a galvanometer based setup was used. Its size was minimized by devising an optical layout comprised of custom-designed scan and GRIN lenses without relay optics. The final dimensions of the rigid endoscope are 2.2 mm diameter with a length of 187 mm. We demonstrate a spatial resolution of 750 nm with a field of view (FoV) of approximately 250 μm . The high imaging quality of the device

is exemplified with images of polymer particles with defined diameters and of human nerves, mouse spinal cord, and mouse adipose tissue.

EXPERIMENTAL RESULTS AND DISCUSSION

The main aim of the research reported here was the implementation of a rigid CARS endoscope providing high spatial resolution and a large FoV while at the same time offering a long effective working distance with a diameter small enough to be applicable, e.g., in neurosurgical interventions. In order to meet these goals, we decided to design an endoscopic unit based on a long and narrow diameter GRIN lens. In the design, we omitted relay optics to realize a compact setup. Since we intended to use our endoscope in medical applications at a later stage, beam scanning with a galvanometer was used for image generation. As a first step, the excitation lasers were delivered via free beam optics with the option of fiber coupling the laser beams to the miniaturized endoscope at a later stage.

CARS microscopy requires the spatial and temporal overlapping of two pulsed excitation beams with the pump laser frequency ω_P and the Stokes laser frequency ω_S . Provided that the frequency difference of the two excitation lasers coincides with the frequency of a vibrational transition of the sample molecules $\omega_{\text{vib}} = \omega_P - \omega_S$, a resonance of $\chi^{(3)}$ will lead to an enhancement of the CARS signal. Our experimental setup is shown in Fig. 1. As a Stokes beam, we used the fundamental of a Nd:YVO₄ laser (1064 nm, repetition rate 76 MHz, pulse duration 6 ps, picoTRAIN, HighQ Laser, Austria) which was used to pump an optical parametric oscillator (OPO; Levante Emerald, APE, Germany). The signal output of the OPO which is tunable between 700 nm and 1000 nm served as a pump beam. Pump and Stokes beams were expanded to a diameter of 7 mm and precisely aligned to overlap in angle and space. An optical delay line is used to achieve temporal overlap of both excitation beams. Both laser beams were spatially scanned as depicted in Fig. 2(a) by using a non-resonant galvanometer mirror (GVS112, Thorlabs, USA). The samples are mounted on a 3D stage (562 series, Newport, USA), and the distance between the sample and the GRIN lens is controlled using a motorized actuator (Z825B, Thorlabs, USA). After focusing onto the sample through the endoscopic unit described below, the CARS signal is collected by using the same unit, descanned by passing through the galvanometer again, separated from the excitation light by using a dichroic beam splitter (HC775LP, Semrock, USA), and detected with a photomultiplier tube (R3869, Hamamatsu, Japan). Images are generated by raster scanning the samples. Shortest pixel dwell times were 8 μ s

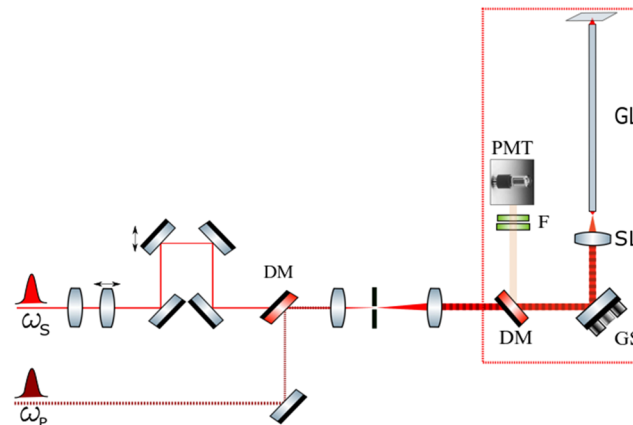


FIG. 1. A frequency doubled Nd:YVO₄ oscillator operating at a repetition rate of 76 MHz pumps an optical parametric oscillator (OPO). The signal output of the OPO tunable between 690 nm and 1000 nm with pulse durations of 6 ps is used as the pump beam. It is combined with residual pump light from the oscillator with a wavelength of 1064 nm serving as the Stokes beam. Both beams are spatially overlapped before coupling into the endoscope head [red box, cf. Fig. 2(a)]. An optical delay line is used to temporally overlap the excitation beams. Both beams are scanned with a galvanometer mirror (GS), before focusing onto the sample with a gradient index lens (GL). The CARS signal is collected by the GRIN lens in a back scattering geometry. It is separated from the excitation light with a dichroic mirror (DM), spectrally filtered (F), and detected with a photomultiplier tube (PMT).

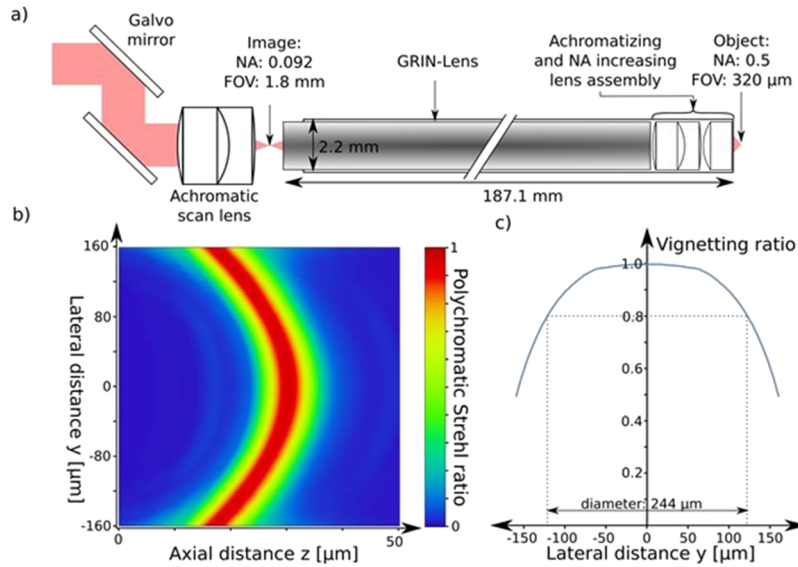


FIG. 2. (a) A non-resonantly driven galvanometer mirror scans a 7 mm diameter beam with a uniform intensity distribution consisting of the pump (803 nm) and Stokes wavelengths (1064 nm). A subsequent achromatic scan lens forms a diffraction limited intermediate image with a diameter of 1.8 mm. The endoscopic unit, hence, projects this intermediate image toward the sample and demagnifies it by a factor of 5.6. The image is not to scale. For (b) and (c), pump and Stokes wavelengths of 803 nm and 1064 nm, respectively, were assumed. (b) Presentation of the simulated linear polychromatic Strehl ratio at the object depending on the lateral distance and axial position in object space shows a diffraction limited performance within the entire FoV and depicts the tolerated field curvature. Vignetting effects are not considered. (c) Simulated vignetting plot shows vignetting effects toward the margin of the FoV. The usable FoV with more than 80% energy transmission is limited to 244 μm .

such that images with a dimension of 500×500 pixels could be recorded within 3.8 s. Please note that the bottleneck of the image acquisition speed in our setup is primarily the readout electronics [sampling rate of the A/D converter (PCIe-6323, National Instruments, USA) and rise time of the amplifier used] and the scan speed of the galvanometer. With the setup described, faster imaging speeds are possible if the CARS signal-to-noise-ratios (SNR) (~ 5.6 for 1 μm size PS beads and ~ 12 for murine adipose tissue) are taken into account. These SNR values are estimated by dividing the mean value of a homogenous high intensity region in the image by the standard-deviation (SD) of the same region.

An important aspect in the design of a CARS endoscope is the avoidance of non-resonant four wave mixing (FWM) generation in the optical system which would deteriorate the achievable sensitivity. While short GRIN lenses have been used previously in CARS and SRS endoscopic measurements,³⁰ the design of longer and more complex GRIN optics requires care to minimize non-resonant background generation in the optical system. The non-resonant FWM signal will mainly originate from common foci of the pump and Stokes beams in the beam path. In order to evaluate the strength of this background under various optical conditions, we performed test measurements with 2.0 mm diameter GRIN-lens of 0.1 numerical aperture (NA) and 0.75 pitch length, length of periodic ray trajectories within the GRIN lens,³³ using different NA optics focusing just behind the front surface of the GRIN-lens (Table I). FWM signals acquired within this experiment are measured in the forward direction.

Our results indicate that the NA of the optics focusing onto the GRIN lens is a decisive factor in the generation of non-resonant background. For this reason, we opted for a custom-designed, achromatized, low NA scan lens with a focal length of $f = 30.0$ mm, a NA of 0.12, and a FoV of 1.8 mm, as depicted in Fig. 2(a). The radii of curvature of the achromatic doublet are from left to right 57.049 mm, 13.432 mm, and -28.78 mm, and the thickness of the flint and crown glass material is 5 mm and 10 mm, respectively. A precise positioning of the scan lens at an axial distance f from the center between the two galvanometer mirrors ensures telecentricity. The custom achromatic scan lens is directly used to focus the lasers close to the entrance pupil of the endoscope, hence omitting

TABLE I. FWM signal intensity of a GRIN lens material of pitch 0.75 doped with Li ions as used in the endoscope as a relay optical element was measured using NIR Apo objectives of 5× NA 0.14, 10× NA 0.26, and 20× NA 0.4 (Mitutoyo, Japan). The FWM signal was measured in the forward direction focusing the excitation laser beams into the GRIN lens. In the last column, the peak count of the FWM signal is given. The measurement with NA 0.07 was done by underfilling the 5× objective. Laser parameters: 1 MHz repetition rate, 35 ps pulse duration pump, 100 ps pulse duration Stokes, temporally overlapping pump and Stokes pulses, 10 mW pump at 796 nm, 40 mW Stokes at 1030 nm, 2850 cm⁻¹ frequency difference of pump and Stokes. A compact spectrometer (HR4000, Ocean Optics) was used. All spectra were normalized to 100 ms acquisition time, and the background has been subtracted. The signal recorded for NA = 0.07 is very close to the noise floor of the instrument. Due to the nonlinear dependence on the signal intensity and due to the phasematching condition, the process starts at a certain threshold NA of ~0.07.

Doped ion	GRIN-NA	Pitch length	Illumination NA	FWM signal (a.u.)
Li ⁺	0.1	0.75	0.07	40
Li ⁺	0.1	0.75	0.14	1160
Li ⁺	0.1	0.75	0.26	5600

the 4-f relay optics of scan and tube lenses as used in table-top microscopes²⁴ in order to significantly shrink the axial length of the overall optical assembly to f only. Simulations predicted a uniformly high optical performance in terms of a polychromatic Strehl ratio exceeding a value of 0.97 within the entire intermediate image. Moreover, experimental misalignments and minor violations of the telecentricity due to the spatial separation of the two scanning mirrors are compensated by a lowered proximal acceptance NA of the GRIN-lens and, hence, the endomicroscopic unit of about 0.09. This unit is placed at an axial distance of 500 μm from the focus of the scan lens which corresponds to the proximal working distance of the GRIN-assembly. The endoscope then projects this intermediate image toward the object while using a demagnification of $m = 5.6$ leading to a distal FoV of 320 μm in diameter. Furthermore, the GRIN-probe magnifies the NA from the intermediate image by about the same factor m to a value of 0.5 at the object, as predicted by the Smith-Helmholtz formula.⁵ A diffraction limited performance is expected by simulations performed at 820 nm within the entire FoV as depicted in Fig. 2(b) which results in the case of linear imaging processes according to the Abbe resolution limit to a lateral and axial FWHM of 0.83 μm and 5.8 μm , respectively. Moreover, we opted for a distal working distance of 30 μm in tissue in the presented simulation and experiment to ensure a low penetration depth and a high optical performance for *in vivo* applications close to the surface of the region of interest. However, in further endomicroscopic probes manufactured within the scope of this project the distal working distance in tissue was adapted to values between 10 μm and 165 μm by grinding and polishing processes of the distal cover plate. A similar diffraction limited performance is achieved by simulations assuming a non-scattering tissue with optophysical properties similar to water. Dispersion measurements of the stand-alone GRIN-lens incorporated inside the endoscopic unit showed a longitudinal chromatic shift of a one-pitch lens of 1.1 μm per nm at 803 nm. An achromatizing and NA increasing subassembly incorporated at the distal end of the probe as depicted schematically in Fig. 2(a) compensates for those longitudinal as well as lateral chromatic aberrations. The second advantage of placing the color correction unit at the distal end of the endoscope is the prevention of a precise overlap of the pump and Stokes beams at intermediate foci within the GRIN-element and hence the reduction in the non-resonant FWM background induced at these locations.

The mechanical dimensions of the probe are designed to obtain a long and thin probe fitting into a standard working channel of a typical rigid endoscope. Therefore, all incorporated optics have an outer diameter of 2.0 mm leading to an overall mechanical diameter of the probe of 2.2 mm and an overall length of 187.1 mm. This length is mainly achieved by incorporating an approximately 1.75 pitch GRIN-relay lens with an acceptance NA of about 0.09. Furthermore, Fig. 2(b) shows the polychromatic Strehl ratio, which is obtained by evaluating the non-coherent superpositions of the monochromatic point-spread-functions (at 803 nm and 1064 nm) at the object for the radial and axial focus positions in object space. The graph points out the diffraction-limited performance within the entire FoV and indicates the tolerated field curvature of the probe of about 13 μm at the margin of the FoV. This plot, however, does not reflect vignetting effects which lead to a decreased performance in terms of efficiency when approaching the margin. This dependence is

depicted in [Fig. 2(c)] and indicates that the FoV, defined as the region in which more than 80% of the excitation energy reaches the sample, is limited to a diameter of 244 μm . The total throughput of the GRIN lens is measured to be at the order of 75% for both wavelengths. Moreover, no change in temporal and spectral pulse characteristics, measured with an autocorrelator (pulseCheck, APE Berlin, Germany) and spectrometer (OceanOptics, USB4000, USA), respectively, is observed after the endoscope.

In order to characterize the optical performance of the whole endoscope, we have performed measurements on well-defined samples consisting of polymer beads as well as on different types of tissue samples from mouse and human. The use of mouse tissue was approved by the animal welfare committee of Saxony, Germany (Regierungspräsidium Dresden, AZ: 24-9168.11-1/2011-39). Human tissue was obtained during routine surgery. The patients gave written consent, and the study was approved by the ethics committee at University Hospital Carl Gustav Carus, Technische Universität Dresden, Germany (EK 323122008).

All signals were recorded in a back-scattering geometry which is the normal mode of operation of an endoscope. In a first set of experiments, we tested the spatial resolution of the endoscope by imaging close packings of polystyrene (PS) beads with a diameter of 1 μm . The sample was about 200 μm thick, and no immersion medium was applied (air spaced). With excitation wavelengths for the pump and the Stokes lasers $\lambda_P = 803 \text{ nm}$ and $\lambda_S = 1064 \text{ nm}$, respectively, and the NA = 0.5 at the distal side of the endoscope, a spatial resolution of 750 nm was achieved. This value was determined by the intensity fit of a single 1 μm PS bead and obtaining its FWHM (Fig. 3). The experimentally achievable FoV can also be estimated from the measurements of densely packed polymer beads on a cover slip. For this sample, we find that the experimental FoV is in very good quantitative agreement with the simulated value of 244 μm . One should note, however, that we have also observed larger FoVs up to 310 μm for samples with thicker structures or stronger CARS signals. Deviations from the simulated values [Fig. 2(c)] are expected due to the cubic dependence of the CARS signal on the excitation intensities and on the fact that the effect of the field curvature [as depicted in Fig. 2(c)] on the CARS signal is more pronounced for thinner structures. The large FoV together with the high spatial resolution is a prerequisite for practical use of the endoscope. Subsequent to the experiments on beads, we tested our setup on thin tissue sections and also on bulk tissue samples. In such experiments, the recording of different imaging modalities is an attractive option to further enhance the information content obtained in the imaging experiments.³⁴ In some experiments, we therefore chose appropriate dichroic filters in the detection path to record the CARS signal (short pass 720/SP; Semrock, USA; ET680-2p8; Chroma, USA; and band pass 650/50 and 630/90; Semrock, USA) or two-photon excited autofluorescence (short pass 720/SP, 775/SP; Semrock, USA; ET680-2p8; Chroma, USA; and band pass 525/50; Semrock, USA; Fig. 4). The images show that the desired high spatial resolution and large FoVs can also be realized under imaging conditions encountered in biomedical experiments.

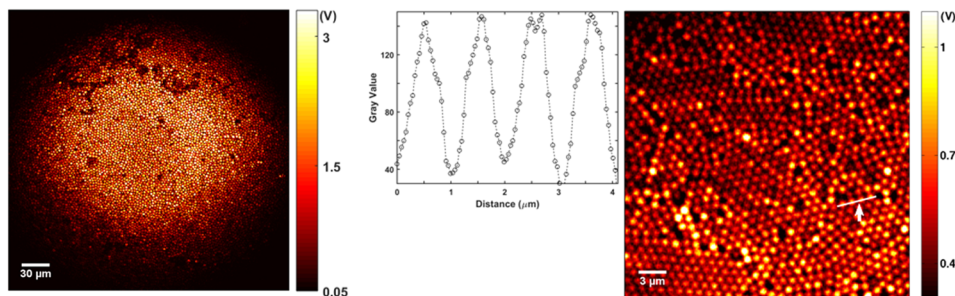


FIG. 3. Left: CARS endoscopic image of 3 μm diameter polystyrene beads dried on a glass coverslip. An overview image indicating the usable FoV. Imaging conditions: power on the sample is 15 mW for each beam (30 mW total power), pixel dwell time is 8 μs averaged over 5 frames, and pixel size is 0.6 μm . Right: zoomed-in view of the close packing of the 1 μm diameter polystyrene beads. The profile plot (inset) over a row of particles (white line in the image). FWHM of an intensity fit of a single 1 μm PS bead indicates the achievable spatial resolution on the order of 750 nm. Imaging conditions: power on the sample is 20 mW for each beam (40 mW total power), pixel dwell time is 8 μs averaged over 5 frames, and pixel size is 0.06 μm .

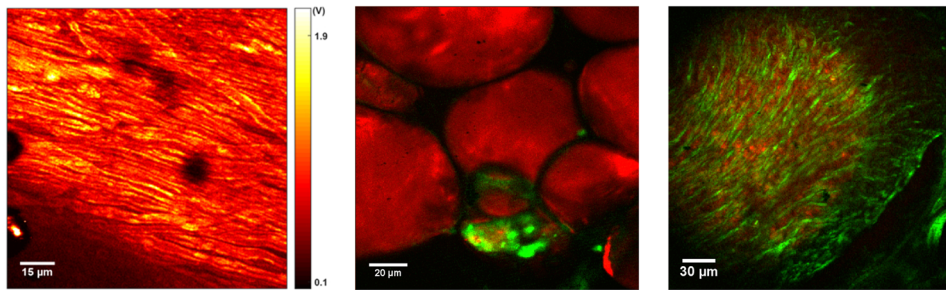


FIG. 4. Left: CARS endoscopic image of a murine spinal cord sample (bulk sample). Individual axons can clearly be distinguished. Imaging conditions: pixel dwell time is $8 \mu\text{s}$ averaged over 5 frames, and pixel size is $0.24 \mu\text{m}$. Middle: CARS (red) and TPEF (green) endoscopic images of murine adipose tissue (bulk sample). Imaging conditions: pixel dwell time is $8 \mu\text{s}$ averaged over 5 frames, and pixel size is $0.3 \mu\text{m}$. Right: CARS (red) and TPEF (green) endoscopic images of a human nervus suralis sample (cryosection). Imaging conditions: pixel dwell time is $8 \mu\text{s}$ averaged over 5 frames, and pixel size is $0.6 \mu\text{m}$. Excitation parameters for CARS were 40 mW at $\lambda_P = 817 \text{ nm}$ and 25 mW at $\lambda_S = 1064 \text{ nm}$ on the bulk samples; 60 mW at $\lambda_P = 817 \text{ nm}$ and 35 mW at $\lambda_S = 1064 \text{ nm}$ on the cryosection sample. The energy difference corresponds to $\Delta\tilde{\nu} = 2841 \text{ cm}^{-1}$. The two-photon excited fluorescence images were recorded with 80 mW total excitation power on the sample for both samples at 817 nm .

While on the one hand, fine structures such as individual axons are readily resolved, large FoVs of roughly $250 \mu\text{m}$ allow the inspection of extended sample areas.

To put the performance of the CARS endoscope described above into perspective, it must be compared with other designs of rigid nonlinear optical endoscopes. Jung and Schnitzler have reported the first rigid, GRIN based endoscope suitable for using one excitation laser beam which suffices for two-photon excited fluorescence and SHG imaging.^{17,18} In connection with galvanometer scanning, these authors report spatial resolutions of slightly more than $1.2 \mu\text{m}$ and a FoV of approximately $120 \mu\text{m}$, however, with optics in which the maximum useable length of the endoscope was 26 mm . The first rigid coherent Raman endoscope was published by Saar and co-workers.³⁰ In this case, a piezo scanner was used for scanning the proximal side of a focusing GRIN lens. In this manner, spatial resolutions of roughly $2 \mu\text{m}$ were achieved with an $80 \mu\text{m}$ diameter FoV. The main drawback of the reported endoscope was the use of a $10 \times 10 \text{ mm}^2$ large detector around the GRIN lens to allow for SRS detection. For CARS imaging alone, a different smaller diameter design could have been employed. Other reports of rigid CARS microscopes concern designs, which are too large in diameter for most scenarios of applications^{1,16} or have optics which are too short.⁴

We thus conclude that the endoscope reported here represents an important step toward the medical application of CARS endoscopy in that it combines unprecedented high spatial resolution and large FoV in a compact setup with narrow diameter and long usable working distance optics. It is planned to integrate the CARS endo-microscope introduced here into a commercially available endoscope which will allow the evaluation of merits of CARS endo-microscopy in clinical environments. In the case of interest to use the CARS-probe in pursuing experiments, Grintech GmbH intends to develop the probe as a product.

ACKNOWLEDGMENTS

The financial support from the German Federal Ministry of Education and Research (BMBF), Verbundprojekt endoCARS, Grant No. 13N13806, is gratefully acknowledged.

¹ Balu, M., Liu, G., Chen, Z., Tromberg, B. J., and Potma, E. O., "Fiber delivered probe for efficient CARS imaging of tissues," *Opt. Express* **18**, 2380–2388 (2010).

² Barad, Y., Eisenberg, H., Horowitz, M., and Silberberg, Y., "Nonlinear scanning laser microscopy by third harmonic generation," *Appl. Phys. Lett.* **70**, 922–924 (1997).

³ Barretto, R. P. J., Messerschmidt, B., and Schnitzer, M. J., "In vivo fluorescence imaging with high-resolution microlenses," *Nat. Methods* **6**(7), 511–512 (2009).

⁴ Belanger, E., Crepeau, J., Laffray, S., Vallee, R., De Koninck, Y., and Cote, D., "Live animal myelin histomorphometry of the spinal cord with video-rate multimodal nonlinear microendoscopy," *J. Biomed. Opt.* **17**, 021107 (2012).

⁵ Born, M. and Wolf, E., *Principles of Optics: Electromagnetic Theory of Propagation Interference and Diffraction of Light* (Pergamon Press, 1980).

- ⁶ Brustlein, S., Berto, P., Hostein, R., Ferrand, P., Billaudeau, C., Marguet, D., Muir, A., Knight, J., and Rigneault, H., "Double-clad hollow core photonic crystal fiber for coherent Raman endoscope," *Opt. Express* **19**, 12562–12568 (2011).
- ⁷ Campagnola, P. J. and Loew, L. M., "Second-harmonic imaging microscopy for visualizing biomolecular arrays in cells, tissues and organisms," *Nat. Biotechnol.* **21**, 1356–1360 (2003).
- ⁸ Débarre, D., Supatto, W., Pena, A. M., Fabre, A., Tordjmann, T., Combettes, L., Schanne-Klein, M. C., and Beaurepaire, E., *Nat. Methods* **3**, 47–53 (2006).
- ⁹ Denk, W., Strickler, J., and Webb, W., "Two-photon laser scanning fluorescence microscopy," *Science* **248**, 73–76 (1990).
- ¹⁰ Ducourthial, G., Leclerc, P., Mansuryan, T., Fabert, M., Brevier, J., Habert, R., Braud, F., Batrin, R., Vever-Bizet, C., Bourghackly, G., Thiberville, L., Druilhe, A., Kudlinski, A., and Louradour, F., "Development of a real-time flexible multiphoton microendoscope for label-free imaging in a live animal," *Sci. Rep.* **5**, 18303 (2015).
- ¹¹ Duncan, M. D., Reintjes, J., and Manuccia, T. J., "Scanning coherent anti-Stokes Raman microscope," *Opt. Lett.* **7**, 350–352 (1982).
- ¹² Freudiger, C. W., Min, W., Saar, B. G., Lu, S., Holtom, G. R., He, C., Tsai, J. C., Kang, J. X., and Xie, X. S., "Label-free biomedical imaging with high sensitivity by stimulated Raman scattering microscopy," *Science* **322**, 1857–1861 (2008).
- ¹³ Freund, I. and Deutsch, M., "Second-harmonic microscopy of biological tissue," *Opt. Lett.* **11**, 94–96 (1986).
- ¹⁴ Fu, L., Jain, A., Cranfield, C., Xie, H. K., and Gu, M., "Three-dimensional nonlinear optical endoscopy," *J. Biomed. Opt.* **12**, 040501 (2007).
- ¹⁵ Göbel, W., Kerr, J. N., Nimmerjahn, A., and Helmchen, F., "Miniaturized two-photon microscope based on a flexible coherent fiber bundle and a gradient-index lens objective," *Opt. Lett.* **29**, 2521–2523 (2004).
- ¹⁶ Hirose, K., Aoki, T., Furukawa, T., Fukushima, S., Niioka, H., Deguchi, S., and Hashimoto, M., "Coherent anti-Stokes Raman scattering rigid endoscope toward robot-assisted surgery," *Biomed. Opt. Express* **9**, 387–396 (2018).
- ¹⁷ Jung, J. C. and Schnitzer, M. J., "Multiphoton endoscopy," *Opt. Lett.* **28**, 902–904 (2003).
- ¹⁸ Jung, J. C., Mehta, A. D., Aksay, E., Stepnoski, R., and Schnitzer, M. J., "*In vivo* mammalian brain imaging using one- and two-photon fluorescence microendoscopy," *J. Neurophysiol.* **92**, 3121–3133 (2004).
- ¹⁹ Knittel, J., Schnieder, L., Buess, G., Messerschmidt, B., and Possner, T., "Endoscope-compatible confocal microscope using a gradient index-lens system," *Opt. Commun.* **188**, 267–273 (2001).
- ²⁰ Legare, F., Evans, C. L., Ganikhanov, F., and Xie, X. S., "Towards CARS endoscopy," *Opt. Express* **14**, 4427–4432 (2006).
- ²¹ Le Harzic, R., Weinigel, M., Riemann, I., König, K., and Messerschmidt, B., "Nonlinear optical endoscope based on a compact two axes piezo scanner and a miniature objective lens," *Opt. Express* **16**, 20588–20596 (2008).
- ²² Lombardini, A., Mytskaniuk, V., Sivankutty, S., Andresen, E. R., Chen, X., Wenger, J., Fabert, M., Joly, N., Louradour, F., Kudlinski, A., and Rigneault, H., "High-resolution multimodal flexible coherent Raman endoscope," *Light: Sci. Appl.* **7**, 10 (2018).
- ²³ Lukic, A., Dochow, S., Bae, H., Matz, G., Latka, I., Messerschmidt, B., Schmitt, M., and Popp, J., "Endoscopic fiber probe for nonlinear spectroscopic imaging," *Optica* **4**, 496–501 (2017).
- ²⁴ Masters, B. R., "Handbook of biological confocal microscopy," *J. Biomed. Opt.* **13**(2), 029902 (2008).
- ²⁵ Messerschmidt, B., McIntyre, B., and Houde-Walter, S. N., "Desired concentration-dependent ion exchange for micro-optic lenses," *Appl. Opt.* **35**, 5670–5676 (1996).
- ²⁶ Myaing, M. T., MacDonald, D. J., and Li, X., "Fiber-optic scanning two-photon fluorescence endoscope," *Opt. Lett.* **31**, 1076–1078 (2006).
- ²⁷ Nandakumar, P., Kovalev, A., and Volkmer, A., "Vibrational imaging based on stimulated Raman scattering microscopy," *New J. Phys.* **11**, 033026 (2009).
- ²⁸ Ploetz, E., Laimgruber, S., Berner, S., Zinth, W., and Gilch, P., "Femtosecond stimulated Raman microscopy," *Appl. Phys. B* **87**, 389–393 (2007).
- ²⁹ Rivera, D. R., Brown, C. M., Ouzounov, D. G., Pavlova, I., Kobat, D., Webb, W. W., and Xu, C., "Compact and flexible raster scanning multiphoton endoscope capable of imaging unstained tissue," *Proc. Natl. Acad. Sci. U. S. A.* **108**, 17598–17603 (2011).
- ³⁰ Saar, B. G., Johnston, R. S., Freudiger, C. W., Xie, X. S., and Seibel, E. J., "Coherent Raman scanning fiber endoscopy," *Opt. Lett.* **36**, 2396–2398 (2011).
- ³¹ Seibel, E. J. and Smithwick, Q. Y., "Unique features of optical scanning, single fiber endoscopy," *Lasers Surg. Med.* **30**, 177–183 (2002).
- ³² Tang, S., Jung, W. G., McCormick, D., Xie, T. Q., Su, J. P., Ahn, Y. C., Tromberg, B. J., and Chen, Z. P., "Design and implementation of fiber-based multiphoton endoscopy with microelectromechanical systems scanning," *J. Biomed. Opt.* **14**, 034005 (2009).
- ³³ Träger, F., *Springer Handbook of Lasers and Optics* (Springer Science & Business Media, 2012).
- ³⁴ Vogler, N., Heuke, S., Bocklitz, T. W., Schmitt, M., and Popp, J., "Multimodal imaging spectroscopy of tissue," *Annu. Rev. Anal. Chem.* **8**, 359–387 (2015).
- ³⁵ Witte, S., Negrean, A., Lodder, J. C., de Kock, C. P., Testa Silva, G., Mansvelter, H. D., and Louise Groot, M., *Proc. Natl. Acad. Sci. U. S. A.* **108**, 5970–5975 (2011).
- ³⁶ Zumbusch, A., Holtom, G. R., and Xie, X. S., "Three-dimensional vibrational imaging by coherent anti-Stokes Raman scattering," *Phys. Rev. Lett.* **82**, 4142–4145 (1999).